



1    Insights into microphysical and optical properties of  
2    typical mineral dust within industrial-polluted snowpack  
3    via wet/dry deposition in Changchun, Northeastern China

4    Tenglong Shi,<sup>1,2,3</sup> Jiayao Wang,<sup>1,3</sup> Daizhou Zhang,<sup>4</sup> Jiecan Cui,<sup>5</sup> Zihang Wang,<sup>2</sup> Yue  
5    Zhou,<sup>2</sup> Wei Pu,<sup>2</sup> Yang Bai,<sup>1,3</sup> Zhigang Han,<sup>1,3</sup> Meng Liu,<sup>6</sup> Yanbiao Liu<sup>6</sup>, Hongbin Xie,<sup>6</sup>  
6    Minghui Yang,<sup>6</sup> Ying Li<sup>7</sup>, Meng Gao<sup>8</sup> and Xin Wang<sup>\*,2,6</sup>

7    <sup>1</sup> State Key Laboratory of Spatial Datum, College of Remote Sensing and  
8    Geoinformatics Engineering, Faculty of Geographical Science and Engineering, Henan  
9    University, Zhengzhou, China, 450046

10    <sup>2</sup> Key Laboratory for Semi-Arid Climate Change of the Ministry of Education, College  
11    of Atmospheric Sciences, Lanzhou University, Lanzhou 730000, China

12    <sup>3</sup> Henan Industrial Technology Academy of Spatiotemporal Big Data (Henan  
13    University), Zhengzhou, 450046 China

14    <sup>4</sup> Faculty of Environmental and Symbiotic Sciences, Prefectural University of  
15    Kumamoto, Kumamoto 862-8502, Japan

16    <sup>5</sup> Zhejiang Development & Planning Institute, Hangzhou 310030, China

17    <sup>6</sup> Key Laboratory of Industrial Ecology and Environmental Engineering (Ministry of  
18    Education, China), School of Environmental Science and Technology, Dalian  
19    University of Technology, Dalian 116024, China

20    <sup>7</sup> Key Laboratory of Atmospheric Environment and Extreme Meteorology, Institute of  
21    Atmospheric Physics, Chinese Academy of Sciences, Beijing, China

22    <sup>8</sup> Department of Geography, Hong Kong Baptist University, Hong Kong, China



1   \* Corresponding author: Xin Wang ([wxin@lzu.edu.cn](mailto:wxin@lzu.edu.cn)).

2   **Abstract.** This study utilizes the computer-controlled scanning electron microscope  
3   software IntelliSEM-EPAS<sup>TM</sup>, combined with K-means cluster analysis and manual  
4   experience, reports for the first time that the dust in the snow accumulation from a  
5   typical industrial city in China is mainly composed of kaolinite-like (36%), chlorite-  
6   like (19%), quartz-like (15%), illite-like (14%), hematite-like (5%), and clay-minerals-  
7   like (4%) and other components. It was also found that the size distribution and aspect  
8   ratio of the dust did not undergo significant changes during dry and wet deposition, but  
9   they exhibited great variability among the different mineral composition groups.  
10   Subsequently, these observed microphysical parameters were used to constrain the  
11   optical absorption of dust, and the results showed that under low (high) snow grain size  
12   scenarios, the albedo reductions caused by dust concentrations of 1, 10, and 100 ppm  
13   in snow were 0.007 (0.022), 0.028 (0.084), and 0.099 (0.257), respectively. These  
14   results emphasize the importance of dust composition and size distribution  
15   characteristics in constraining snowpack light absorption and radiation processes.

16



## 1 **1 Introduction**

2 Snow constitutes a crucial component of the terrestrial cryosphere, covering  
3 approximately 40% of the global land area, with a maximum extent of around 45  
4 million square kilometers (Hall et al., 1995; Lemke et al., 2007). It is predominantly  
5 found in polar and high-latitude regions, as well as mountainous areas at mid-to-low  
6 latitudes, exhibiting significant temporal and spatial variability due to seasonal changes  
7 (Tan et al., 2019; Thackeray et al., 2016; Zhu et al., 2021). Current research indicates  
8 that light-absorbing aerosols in the atmosphere (e.g. black carbon, brown carbon, and  
9 dust) are eventually deposited on the snow surface or glaciers through atmospheric  
10 diffusion, transport, and dry/wet deposition processes (Doherty et al., 2010; Gilardoni  
11 et al., 2022; Kuchiki et al., 2015). This alters the single optical properties of the  
12 snowfield, enhances the absorption of solar radiant energy, and reduces the albedo of  
13 the snow and ice surface, thereby accelerating snowmelt and altering the water cycle,  
14 and exerting a nuanced yet pivotal role in regional climate dynamics (Hadley and  
15 Kirchstetter, 2012; Hansen and Nazarenko, 2004; Kang et al., 2020; Skiles et al., 2018).  
16 Hence, it emerges as a critical determinant impacting both regional and global climate  
17 change.

18 Extensive observational evidences highlighted significant reductions in the extent and  
19 duration of snow cover across the Northern Hemisphere, particularly notable in high-  
20 latitude and mountainous regions due to global warming (Bormann et al., 2018;  
21 Derksen and Brown, 2012; Mote et al., 2018; Pulliainen et al., 2020; Zeng et al., 2018).  
22 Currently, the duration of Northern Hemisphere snow cover is decreasing by



1 approximately 5-6 days per decade (Dye, 2002), with Arctic June snow cover  
2 diminishing at a rate of 13.6% per decade (Derksen and Brown, 2012; Derksen et al.,  
3 2017). Regions like the western Tibetan Plateau and Australia have experienced snow  
4 cover retreat rates ranging from 11% to 30% per decade (Bormann et al., 2012;  
5 Immerzeel et al., 2009), while the onset of snowmelt in the western United States has  
6 advanced by 6-26 days since the mid-1970s (Hall et al., 2015). Dust, a prevalent aerosol  
7 type in the Earth-atmosphere system, has garnered significant scientific attention due  
8 to its role in accelerating ice and snow melt (Bryant et al., 2013; Dong et al., 2020;  
9 Kaspari et al., 2015; Painter et al., 2012). Réveillet et al. (2022) reported an 8-12 day  
10 earlier average snowmelt in the French Alps and the Pyrenees due to dust presence  
11 during 1979-2018. Zhang et al. (2018) found that dust reduced snow albedo in the  
12 southern Tibetan Plateau by approximately  $0.06 \pm 0.004$ , equivalent to 30% of the  
13 albedo reduction caused by black carbon. Sarangi et al. (2020) further demonstrated  
14 dust's primary contribution to snow darkening above 4000 m altitude in the Tibetan  
15 Plateau, surpassing that of black carbon in influencing regional ice and snow melt.  
16 Whereas Xing et al. (2024) and Winton et al. (2024) also highlighted the remarkable  
17 contribution of dust events to the snow darkening of the Asian High Mountains and the  
18 Southern Alps, respectively. Moreover, Hao et al. (2023) projected a decrease in black  
19 carbon deposition on ice and snow under future emission scenarios, while anticipating  
20 heightened dust emissions and deposition fluxes driven by climate change-induced land  
21 use changes (Neff et al., 2008), frequent wildfires (Yu and Ginoux, 2022), and increased  
22 drought (Huang et al., 2016).. Consequently, dust's impact on ice and snow melt is



1 expected to intensify markedly.

2 Previous studies have focused on investigating the concentration of dust in snow and

3 its related radiative effects, neglecting the impact of the microphysical properties of

4 dust on its optical absorption (Bryant et al., 2013; Reynolds et al., 2020; Xie et al.,

5 2018). In fact, the physical and chemical properties of mineral dust aerosols, including

6 their particle size distribution (PSD), composition, mixing state, and shape, determine

7 their optical properties (Chou et al., 2008; Colarco et al., 2014; Fountoulakis et al., 2024;

8 Haapanala et al., 2012; Shi et al., 2022). Dong et al. (2020) compared the volume-size

9 distribution of dust deposition in ice and snow in western China and the Arctic, finding

10 significant differences in the median particle size of dust, and showing that the particle

11 size decreases with altitude in various remote regions except for the remote Arctic and

12 Antarctic regions. Wang et al. (2023) used intelligent scanning electron microscopy to

13 obtain typical PSD of dust in snow in Changchun. Additionally, related dust studies in

14 the atmosphere have confirmed the complex variability of dust mineral composition.

15 For example, in the case of dust aerosols from the Sahara Desert collected in Izana,

16 Spain, in the summer of 2005, it was found that they were mainly composed of silicates

17 (64%) and sulfates (14%), with small amounts of carbonaceous materials (9%), quartz

18 (6%), calcium-rich particles (5%), hematite (1%), and soot (1%) (Kandler et al., 2007).

19 In contrast, dust particles collected in Beijing, China, during an Asian dust storm were

20 primarily composed of clay minerals (35.5wt%, by weight percentage), quartz

21 (30.3wt%), and calcite (14.0wt%), followed by feldspar (8.7wt%), pyrite (1.0wt%), and

22 hornblende (0.4wt%), along with noncrystalline materials (10.1wt%) (Shi et al., 2005).



1   Panta et al. (2023) conducted detailed field measurements using electron microscopy  
2   in the Sahara Desert of Morocco, reporting the statistical characteristics of the single-  
3   particle composition, size, mixing state, and aspect ratio of newly emitted mineral dust.  
4   To date, no studies have comprehensively analyzed the composition, size, and  
5   morphology of dust in snow or clarified the interrelationships among these  
6   characteristics. This lack of understanding significantly limits accurate assessments of  
7   the optical properties and radiative effects of dust in ice and snow (Flanner et al., 2021;  
8   He et al., 2024).  
9   Based on a field snow observation experiment conducted in Changchun, northeastern  
10   China, in November 2020, this study utilized intelligent scanning electron microscopy  
11   with an energy-dispersive X-ray analyzer to investigate in detail the composition, size,  
12   and morphological characteristics of dust during dry and wet deposition. These  
13   statistically significant parameters were subsequently used to constrain the complex  
14   refractive index and optical absorption inversion of dust, providing more accurate dust  
15   optical parameter inputs for snow radiative transfer models, and enhancing the accuracy  
16   of climate effect assessments of dust in snow.

## 17   **2 Methods**

### 18   **2.1 Snow sample collection and analysis**

19   Our previous study has detailed the snow field experiment conducted in Changchun  
20   (Wang et al., 2023). During and after a heavy snowfall from November 19 to December  
21   17, 2020, we collected snow samples every two days, yielding a total of one fresh



1 snowfall sample (wet deposition) and 15 aged surface snow samples (dry deposition).  
2 This study selected five samples for measurement and analysis at intervals of 6-8 days,  
3 including one wet deposition sample (D1) and four dry deposition samples (D7, D15,  
4 D23, and D29; "D" denotes days). Briefly, the selected snow samples were melted at  
5 room temperature, and an appropriate volume of the snow solution was taken based on  
6 the cleanliness of the snow sample. The solution was filtered through a polycarbonate  
7 membrane with a diameter of 25 mm and a pore size of 0.1  $\mu\text{m}$  to separate the particles.  
8 The membrane was then transferred to a storage box and dried in a desiccator. Prior to  
9 analysis, a filter membrane approximately 0.5  $\text{cm}^2$  was cut and gold-plated. The  
10 samples were placed in the electron microscope sample chamber for vacuum processing,  
11 and data were collected and analyzed using the Environmental Particle Analysis  
12 Software (IntelliSEM-EPAS<sup>TM</sup>) of the intelligent scanning electron microscope. The  
13 IntelliSEM-EPAS<sup>TM</sup> system automatically scans multiple matrix areas within the field  
14 of view. By collecting backscattered signals from the scanning electron microscope and  
15 comparing the image signal intensity with preset threshold levels, particles are detected.  
16 Upon detection, the system automatically records the morphology images and positions  
17 of the particles on the polycarbonate membrane and utilizes EDS technology to analyze  
18 the relative content of 24 chemical elements (C, O, F, Na, Mg, Al, Si, P, S, Cl, K, Ca,  
19 Ti, V, Cr, Mn, Fe, Co, Ni, Cu, Zn, As, Br, Rh, Pd, Ag, Ba, Pt, and Pb) in the particles.  
20 This process rapidly generates high-definition images and energy spectrum data for  
21 each particle (thousands of particles per hour). Additionally, IntelliSEM-EPAS<sup>TM</sup>  
22 provides detailed measurements of the maximum and minimum diameters, average



diameter, particle projection area, roundness, and aspect ratio of the particles (Zhao et al., 2022). Compared to manually operated scanning electron microscope experiments, the IntelliSEM-EPAS<sup>TM</sup> system has the advantages of intelligent control and fast analysis speed, allowing for the acquisition of a large amount of environmental particle information in a short time, including detailed data on particle concentration levels, morphology characteristics, and component content across arbitrary size ranges, thereby providing data support for big data analysis of particle micro-morphology characteristics and physicochemical properties.

## 2.2 Dust microphysical properties derived from IntelliSEM-EPAS<sup>TM</sup>

Based on the IntelliSEM-EPAS<sup>TM</sup> system, this study obtained the geometric information and energy spectrum data of about 4,000-5,000 particles in each sample, aiming to reveal the statistical characteristics of the microphysical properties of insoluble particles in snow. Specifically, according to Kandler et al. (2007), particles with a relative mass proportion of C and O elements exceeding 95% were roughly classified as carbonaceous particles. Then, for all remaining particles, the elemental index of each element other than C and O was calculated. Based on single-particle composition quantification, the elemental index of element X is defined as the atomic ratio of the concentration of the considered element to the sum of the concentrations of the quantified elements (Panta et al., 2023).

$$|X| = \frac{X}{(Na+Mg+Al+Si+P+S+Cl+K+Ca+Ti+V+Cr+Mn+Fe+Co+Ni+Cu+Zn+Sn+Ba+Pb)} \quad (1)$$

The elemental symbol indicates the relative contribution measured for each particle (in atomic percent). Using the obtained elemental indices and combining K-Means





1 clustering algorithms and manual experience, these non-carbonaceous particles were  
 2 classified (Kandler et al., 2007; Panta et al., 2023; Zhao et al., 2022). The main principle  
 3 of the K-means clustering algorithm is to use the k-means algorithm to classify particles  
 4 with similar chemical compositions into 30 types based on the elemental index of each  
 5 element, and then, according to relevant research and manual experience classification  
 6 principles of EDS spectra, classify the 30 types into 12 mineral phases, with particle  
 7 categories named after their most common chemical composition, including quartz-like,  
 8 hematite-like, rutile-like, kaolinite-like, chlorite-like, illite-like, hematite-like, clay-  
 9 minerals-like etc. The size distribution of different types of particles is described using  
 10 a normal distribution, specifically expressed as (Li et al., 2021; Flanner et al., 2021):

$$11 \quad n_r = \frac{dN}{dr} = \sum_{i=1}^n \frac{N_i}{\sqrt{2\pi}r\ln(\sigma_i)} \exp \left\{ -\frac{1}{2} \left[ \frac{\ln(r) - \ln(r_i)}{\ln(\sigma_i)} \right]^2 \right\} \quad (2)$$

12 where  $N_i$  is the total number of particles per unit volume in the  $i$ -th size mode,  $r_i$  is  
 13 the mean radius, and  $\sigma_i$  is the geometric standard deviation. These parameters can be  
 14 fitted from the measured data. Similarly, the aspect ratio (AR) of particles is also  
 15 expressed as a normal distribution function (Panta et al., 2023):

$$16 \quad n_{AR} = \frac{dN}{dAR} = \sum_{i=1}^n \frac{N_i}{\sqrt{2\pi}AR\ln(\sigma_i)} \exp \left\{ -\frac{1}{2} \left[ \frac{\ln(AR) - \ln(AR_i)}{\ln(\sigma_i)} \right]^2 \right\} \quad (3)$$

### 17 **2.3 Dust light absorption and snow albedo calculation**

18 Based on the proportion of different mineral phases in the dust, the effective volume  
 19 refractive index ( $m_{eff}$ ) of mineral mixtures in snow aerosols was calculated using the  
 20 effective medium approximation (EMA) method. Specifically, for binary mixtures, the  
 21 effective complex refractive index under EMA-Bruggeman approximation can be  
 22 written as (Kahnert, 2015):



$$m_{\text{eff}} = \sqrt{\frac{1}{4}[m_1^2(2-3f) + m_2^2(3f-1)] + \sqrt{\left[\frac{1}{16}[m_1^2(2-3f) + m_2^2(3f-1)]^2 + \frac{1}{2}m_1^2m_2^2\right]}}$$
(4)

where  $m_1$  is the complex refractive index of the background matrix,  $m_2$  is the complex refractive index of the inclusions, and  $f$  is the volume fraction of the inclusions. The effective complex refractive index for multicomponent mixtures can be obtained by repeating the above process. The refractive indices of different minerals used in this study were obtained from the spectral refractive index dataset of the main mineral components and chemical compositions provided by Zhang et al. (2024). For more detailed information about the dataset, refer to Zhang et al. (2024). Subsequently, using the effective complex refractive indices of dust constrained by observations, size distribution, and aspect ratio (AR) data, we calculated the mass absorption coefficient, single scattering albedo, and asymmetry factor of different types of dust particles using the MOPSMAP program package (Gasteiger and Wiegner, 2018). The MOPSMAP model is a comprehensive aerosol optical property model combining T-matrix, Mie scattering theory, and geometric optics, widely used in calculating complex aerosol optical parameters (Kanngiesser and Kahnert, 2021; Shi et al., 2022).

The simulation of snow albedo was executed by our team's developed the Spectral Albedo Model for Dirty Snow (SAMDS) (Wang et al., 2017), which has been applied in many studies (Shi et al., 2021; Li et al., 2021). Specifically, the albedo of a snow-covered field containing dust under clear sky conditions can be expressed as:



$$R_d(\lambda) = \exp \left( -4 \sqrt{\frac{8\pi B R_{ef} k(\lambda)}{9\lambda(1-g)} + \frac{2\rho_{ice} R_{ef}}{9(1-g)} MAC_{Dust} \cdot C_{Dust} \cdot \frac{3}{7} (1 + 2 \cos(v_0))} \right) \quad (5)$$

where  $\lambda$  is the wavelength in  $\mu\text{m}$ ;  $v_0$  is the solar zenith angle;  $k(\lambda)$  is the imaginary part of the complex refractive index of ice.  $\rho_{ice}$  and  $R_{ef}$  represent the density and effective radius of snow grains (in  $\mu\text{m}$ ), respectively;  $g$  is the asymmetry factor of snow grains (weighted average of the scattering angle cosine);  $B$  is a factor related only to the shape of the snow grains.  $MAC_{Dust}$  is the mass absorption coefficient of dust, and  $C_{Dust}$  is the concentration of dust particles in the snow. Here we used  $B = 1.27$  and  $g = 0.89$  to characterize spherical snow grains (Wang et al., 2017).

### 3 Results

#### 3.1 The composition of dust in seasonal snow

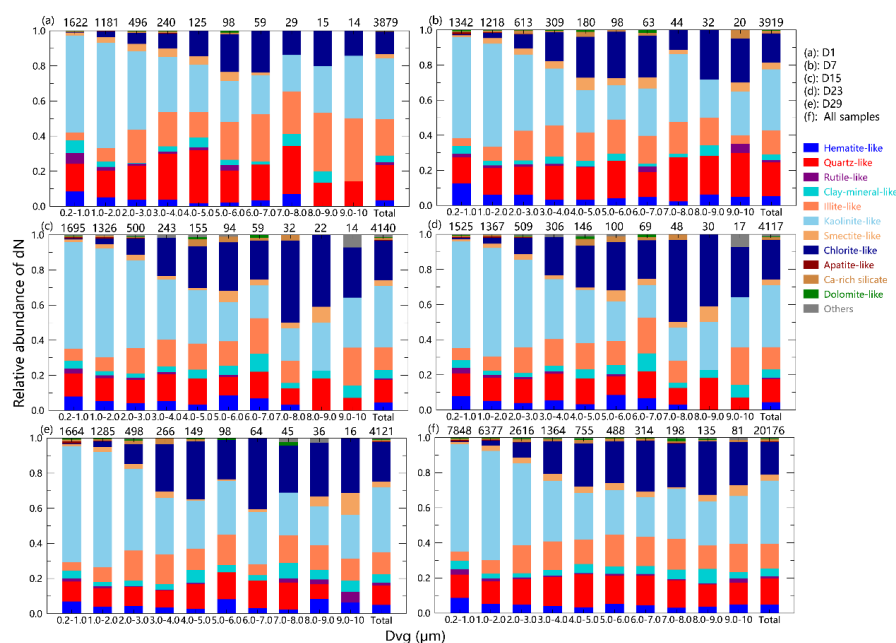
The composition of dust determines its complex refractive index, which is crucial for studying the radiative effects of dust (Reynolds et al., 2020; Lee et al., 2020). This study identified a total of 12 mineral components, including hematite-like, quartz-like, rutile-like, clay-mineral-like, illite-like, kaolinite-like, smectite-like, chlorite-like, apatite-like, Ca-rich silicates, domolite-like, and others. However, it is important to handle this classification scheme with caution, as each particle may consist of different minerals, which may have variable or ambiguous compositions. Therefore, the groups used cannot uniquely identify minerals but rather indicate the most likely minerals matching the particle composition. This is reflected in the suffix "-like" used in the group naming scheme. Given the existence of other potential identification methods, each with its own



1 advantages and limitations, the complete dataset generated and used in this study can  
2 be utilized for future research. Figure 1 (Figure S1) shows the number (mass) relative  
3 proportions of different mineral components in dry and wet deposition snow samples  
4 at different size resolutions, indicating significant trends observed among different  
5 particle groups with changes in size categories. For all samples, kaolinite-like is the  
6 most abundant, present in all size ranges, with its abundance decreasing with increasing  
7 size. Quartz-like particles have nearly similar abundance in each size category  
8 (approximately 10%-20%), which is higher than the values reported by Panta et al.  
9 (2023) for dust from Morocco (approximately 5%). Similarly, clay-minerals-like are  
10 evenly distributed across each size category, accounting for about 4% of the relative  
11 abundance. Hematite-like exhibits similar relative abundances, but its contribution  
12 decreases with increasing particle size, and its strong light-absorbing properties have  
13 drawn widespread attention (Li et al., 2024; Zhang et al., 2015; Moteki et al., 2017). In  
14 contrast, chlorite-like's relative contribution increases with increasing size, with an  
15 average abundance of approximately 20%. It is noteworthy that the relative abundance  
16 of illite-like is higher in wet deposition samples than in dry deposition samples, possibly  
17 due to K-rich illite, considered one of the most effective ice nucleation sources found  
18 among different mineral components in dust (Atkinson et al., 2013; Harrison et al.,  
19 2022). Additionally, the relative abundance of quartz-like in dry deposition samples is  
20 significantly lower than in wet deposition samples, which is closely related to the  
21 migration process of quartz-like particles in snow. Table S1 provides the relative  
22 proportions of different mineral components within the measured size range (0.2-10



1  $\mu\text{m}$ ). Overall, dust in Changchun snow is primarily composed of kaolinite-like (36%),  
 2 chlorite-like (19%), quartz-like (15%), illite-like (14%), hematite-like (5%), and clay-  
 3 minerals-like (4%) and other components. In comparison, Shi et al. (2005) reported  
 4 mineralogical properties of Asian dust primarily consist of clay minerals (35.5wt%, by  
 5 weight percentage), quartz (30.3wt%), and calcite (14.0wt%), followed by feldspar  
 6 (8.7wt%), pyrite (1.0wt%), and hornblende (0.4wt%). For the Middle East, Prakash et  
 7 al. (2016) reported relative mass abundances of clay minerals ranging from 45% to 75%,  
 8 plagioclase from 5% to 54%, and quartz from 0.1% to 10.2% as major components.

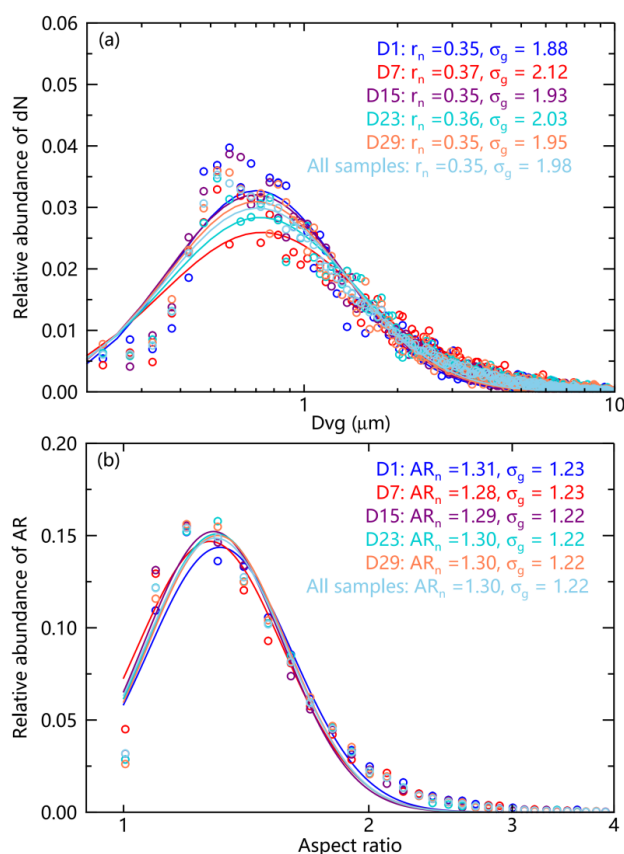


9 **Figure 1.** Size-resolved number abundance of different particle groups for D1 sample  
 10 (a), D7 sample (b), D15 sample (c), D23 sample (d), D29 sample (e), and All samples  
 11 (f). The numbers on top represent total particle counts in the given size bin.

### 13 3.2 Size distribution and aspect ratio of dust in seasonal snow



1 Particle size is a key factor influencing the light-absorbing properties of dust, which has  
2 received widespread attention in field observations, numerical models, and satellite  
3 remote sensing (Castellanos et al., 2024; González-Flórez et al., 2023; Song et al.,  
4 2022). Figure 2a illustrates the size distribution characteristics of dust particles  
5 collected from snow samples at different periods, indicating that the peak particle size  
6 of dust during dry deposition did not vary significantly. All samples exhibited similar  
7 size distributions, with geometric mean radii ranging from 0.35 to 0.37  $\mu\text{m}$  and  
8 geometric standard deviations from 1.88 to 2.12, comparable to findings reported in  
9 other studies (Kok, 2011; Di Mauro et al., 2015; Kok et al., 2017). Interestingly,  
10 significant differences in size spectra were observed among different mineral  
11 components (Figure S2 and Table S2), considering only the cases where the fitted  
12 values passed significance tests. Chlorite-like showed the largest size spectrum, with a  
13 median radius reaching 1.32  $\mu\text{m}$ , significantly higher than smectite-like, the second  
14 largest with a median radius of 0.57  $\mu\text{m}$ . Illite-like exhibited a broader range of sizes  
15 across different snow samples, ranging from 0.38 to 0.59  $\mu\text{m}$ . Kaolinite-like and quartz-  
16 like particles had similar size distributions, with median radii of approximately 0.36  
17  $\mu\text{m}$ , although the geometric standard deviation of the former was slightly lower than  
18 that of the latter. These two components, due to their high proportions, largely  
19 determine the overall size distribution characteristics of dust. Despite hematite having  
20 the smallest size (0.29  $\mu\text{m}$ ), its study is of significant interest due to its strong light-  
21 absorbing properties (Formenti et al., 2014; Go et al., 2022).



1

2 **Figure 2.** Relative abundances of (a) logarithmic dust size number distributions  $dN/$   
 3  $(d\log D_p)$  and (b) logarithmic dust AR number distributions  $dN/ (d\log AR)$  for different  
 4 snow samples.  $D_{vg}$ : particle diameter of dust in snow,  $r_n$ : the number median radius,  
 5  $\sigma_g$ : the geometric standard deviation.

6 Aspect ratio (AR) is another critical geometric parameter of dust particle that affects  
 7 their light-absorbing properties (Botet and Rai, 2013; Haapanala et al., 2012; Huang et  
 8 al., 2023). Figure 2b describes the spectral distribution of aspect ratios of dust particles  
 9 in dry and wet deposition samples. Similar to the size results, the aspect ratio of dust  
 10 particles during dry and wet deposition did not show significant variations, with all



1 samples displaying similar spectral distributions. The geometric mean values ranged  
2 from 1.28 to 1.31, with geometric standard deviations from 1.22 to 1.23. These results  
3 are slightly lower than those reported in atmospheric dust studies, such as  
4 measurements of dust from Morocco and Asia with AR values of 1.46 and 1.40,  
5 respectively (Kandler et al., 2009; Okada et al., 2001). During the Fennec campaign in  
6 central Sahara, a median AR of 1.3 was found (Rocha-Lima et al., 2018), and  
7 measurements of dust particles collected in the Sahara air layer and marine boundary  
8 layer during the AERosol Properties-Dust (AER-D) period showed median AR values  
9 of 1.3-1.44 for particles ranging from 0.5 to 5  $\mu\text{m}$  and 1.30 for particles from 5 to 10  
10  $\mu\text{m}$ , and 1.51 for particles from 10 to 40  $\mu\text{m}$  (Ryder et al., 2018). Furthermore, we also  
11 explored the spectral characteristics of aspect ratios of different mineral components  
12 (Figure S3 and Table S3). Unlike the size distribution, although there are differences in  
13 aspect ratios among different components, the variation range is not large. Most mineral  
14 component groups have similar median AR values of 1.30, except for goethite and clay  
15 minerals, which have the lowest median AR of 1.25 and the highest median AR of 1.37,  
16 respectively. The AR of the same mineral component group shows no significant  
17 differences among different samples. Additionally, we found that AR is generally  
18 independent of particle size and type (Figure S4), consistent with the results of Panta et  
19 al. (2023).

### 20 **3.3 Dust light absorption and its effects on snow albedo**

21 The refractive index of various mineral components exhibits significant variation.  
22 Figure S5 illustrates the complex refractive indices (both real and imaginary parts) of

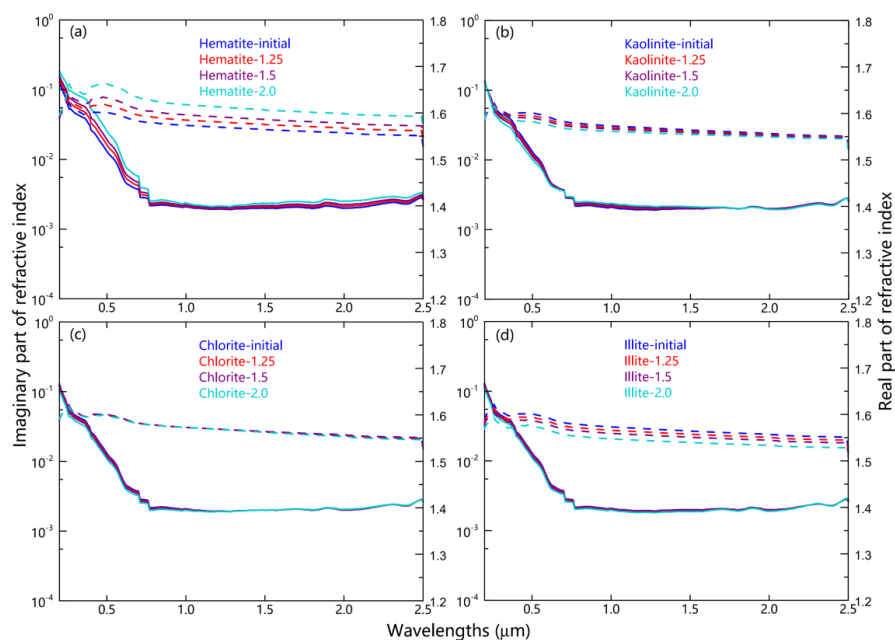




1 the eight principal mineral component groups identified in this study. The imaginary  
2 parts, indicative of absorption, vary by up to six orders of magnitude. Hematite shows  
3 the highest imaginary part of the complex refractive index, indicating the strongest  
4 light-absorbing properties, while quartz displays the smallest, indicating the weakest.  
5 The complex refractive indices of kaolinite, illite, chlorite, and smectite present  
6 relatively similar values, suggesting minimal variation in their light-absorbing  
7 properties. Based on the complex refractive index database of mineral component  
8 groups and combined with volume relative proportions under observational constraints,  
9 an effective medium approximation method is used to obtain the effective complex  
10 refractive index of dust in snow. Additionally, to assess the impact of different mineral  
11 component groups on the effective complex refractive index, we adjusted the initial  
12 volume proportions of hematite, kaolinite, chlorite, and illite by factors of 1.25, 1.50,  
13 1.75, and 2.0, respectively, while keeping the relative proportions of other components  
14 unchanged, and finally normalizing the proportions of all components. Figure 3  
15 illustrates the variation in the effective complex refractive index of dust with  
16 wavelength under these scenarios, focusing on the imaginary parts related to absorption.  
17 Overall,  $k_{\text{dust}}$  is distributed within a narrow range ( $\sim 0.001$ – $0.01$ ), gradually decreasing  
18 with increasing wavelength in the UV and VIS bands, and then stabilizing in the NIR  
19 band, comparable to values reported in other literature. Notably, an increase in the  
20 relative proportion of hematite leads to a significant rise in  $k_{\text{dust}}$ , especially in the visible  
21 spectrum. Conversely, increases in the relative proportions of kaolinite, chlorite, and  
22 illite cause a slight decrease in  $k_{\text{dust}}$ , due to the reduced relative proportion of hematite



1 after normalization.

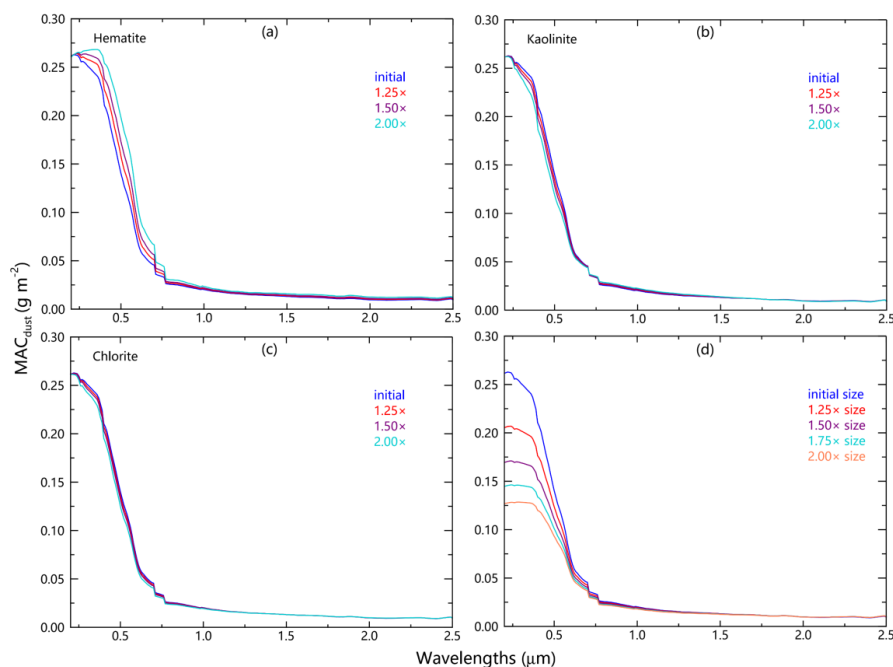


2  
 3 **Figure 3.** Complex spectral refractive indices of dust mixtures in scenarios with  
 4 different composition group percentages. The solid and dashed lines in the diagram  
 5 represent the imaginary and real parts, respectively. The default average volume  
 6 fraction of each mineral group is 35.6% Kaolinite, 19.4% Chlorite, 15.2% Quartz, 14.6%  
 7 Illite, 4.5% Hematite, 3.1% Smectite, and 1.1% Rutile. (a), (b), (c), and (d) represent  
 8 the effects of changes in the proportion of hematite, kaolinite, chlorite, and illite,  
 9 respectively.

10 Furthermore, incorporating observed dust size distribution and AR spectra  
 11 characteristics, we calculated the mass absorption cross-section ( $MAC_{dust}$ ), as shown in  
 12 Figure 4. Similar to  $k_{dust}$ ,  $MAC_{dust}$  is distributed within a narrow range ( $\sim 0$ – $0.3 \text{ m}^2/\text{g}$ ),  
 13 gradually decreasing with increasing wavelength in the UV and VIS bands, and



1 approaching stability ( $\sim 0$ ) at wavelengths greater than 1000 nm. An increased relative  
 2 proportion of hematite enhances  $MAC_{dust}$  in the visible spectrum. For instance,  
 3 doubling the relative proportion of hematite raises  $MAC_{dust}$  at 500 nm from 0.14  $m^2/g$   
 4 to 0.19  $m^2/g$ . However, changes in the relative proportions of kaolinite and chlorite have  
 5 minimal effects on  $MAC_{dust}$ , consistent with the results for  $k_{dust}$ . Additionally, an  
 6 increase in  $R_{dust}$  significantly reduces  $MAC_{dust}$  in the UV and VIS bands, weakening its  
 7 spectral dependence. For example, when  $R_{dust}$  is increased by factors of 1.25, 1.5, and  
 8 2.0,  $MAC_{dust}$  at 300 nm decreases by 20% (0.20  $m^2/g$ ), 33% (0.17  $m^2/g$ ), and 48% (0.13  
 9  $m^2/g$ ), respectively, and at 500 nm, it decreases by 12% (0.12  $m^2/g$ ), 21% (0.11  $m^2/g$ ),  
 10 and 34% (0.09  $m^2/g$ ).



11  
 12 **Figure 4.** Spectral variations in the dust mass absorption cross-sections (MACs) for  
 13 different simulation scenario: (a) Hematite, (b) Kaolinite, (c) Chlorite, and (d) Size.



1 Here the dust aspect ratio is fixed at 1.3.

2 Figure 5a illustrates the impact of changes in the relative proportion of hematite on the

3 spectral snow albedo, considering scenarios with low, medium, and high dust loads in

4 snow, assuming a snow particle size of 500  $\mu\text{m}$  (medium scenario). It can be observed

5 that changes in spectral albedo due to variations in dust concentration and composition

6 proportions generally occur in the visible light spectrum, while the near-infrared (NIR)

7 spectrum is primarily influenced by the microphysical properties of snow particles

8 themselves (Gardner and Sharp, 2010; He and Flanner, 2020), thus unaffected by dust

9 concentration and composition proportions. Specifically, spectral albedo decreases in

10 the UV and visible light (UV-Vis) bands with increasing dust concentration, with a

11 further decrease observed with rising proportions of hematite. Similar to Figure 5a,

12 Figure 5b describes changes in spectral albedo of snow under different dust particle

13 sizes, showing that increasing dust particle size can mitigate the decline in spectral

14 albedo in the visible light spectrum, which is more pronounced in high dust load

15 scenarios. For example, doubling the dust particle size increases the spectral albedo

16 (300 nm) from 0.946, 0.840, and 576 to 0.961, 0.882, and 0.673 for dust concentrations

17 of 1, 10, and 100 ppm in snow, respectively. Figures 5c and 5d respectively illustrate

18 the effects of changes in the relative proportion of hematite and dust particle size on the

19 reduction in snow albedo, considering three snow particle size scenarios. Specifically,

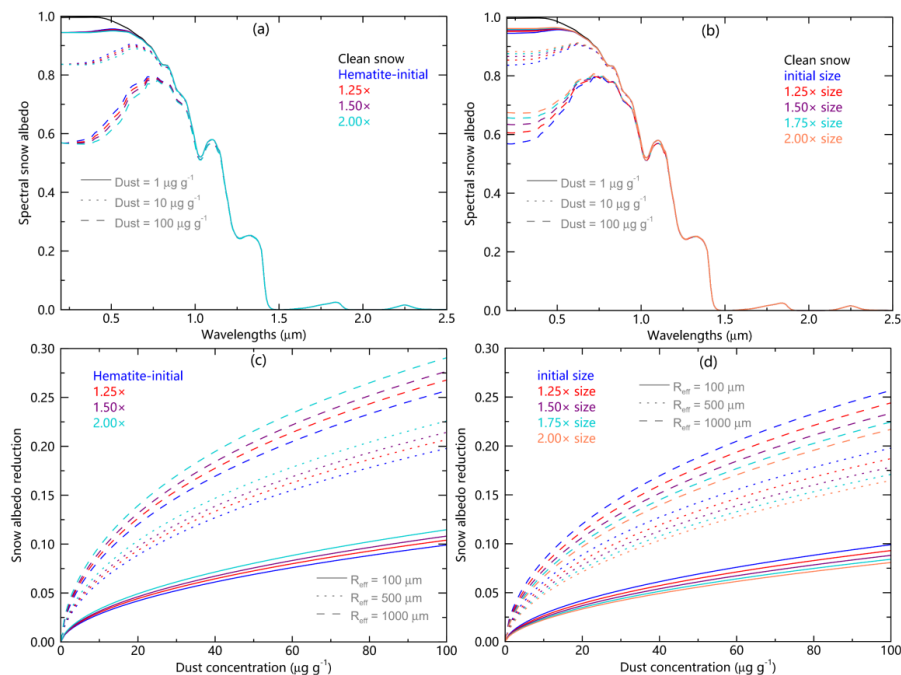
20 the reduction in albedo increases with increasing dust concentration and snow particle

21 size, further exacerbated by an increase in the proportion of hematite, especially in high

22 dust concentration and snow particle size scenarios. Conversely, an increase in dust



1 particle size reduces the reduction in albedo, and increases in dust concentration and  
 2 snow particle size can further amplify this effect. For instance, in low (high) snow  
 3 particle size scenarios, increasing the proportion of hematite increases the reduction in  
 4 albedo caused by dust concentrations of 1, 10, and 100 ppm in snow from 0.007 (0.022),  
 5 0.028 (0.084), and 0.099 (0.257) to 0.008 (0.026), 0.033 (0.098), and 0.115 (0.291).  
 6 Conversely, increasing the dust particle size reduces the reduction in albedo caused by  
 7 dust concentrations of 1, 10, and 100 ppm in snow to 0.005 (0.017), 0.022 (0.066), and  
 8 0.081 (0.217). These results emphasize the complex effects of dust composition,  
 9 particle size, concentration, and snow particle size on snow albedo.



10 **Figure 5.** (a) Spectral snow albedo in the wavelength range of 0.2–2.5  $\mu\text{m}$  for different  
 11 dust concentrations and hematite percentages, with assumed snow radii of 500  $\mu\text{m}$ . (b)  
 12 Spectral snow albedo for different dust concentrations and sizes. (c) Broadband snow  
 13 albedo reduction for different dust concentrations and sizes.



1 albedo reduction as a function of dust concentration for different hematite percentages  
2 and snow grain radii (100, 500, and 1,000  $\mu\text{m}$ ). (d) Similar to (c), but hematite  
3 percentage is replaced with dust size.

#### 4 **4 Summary and discussion**

5 This study employed CCSEM technology to quantitatively analyze insoluble  
6 particulate matter in snow in Changchun, ranging from 0.2 to 10  $\mu\text{m}$ , and identified 12  
7 mineral component groups through K-means cluster analysis and empirical  
8 identification. The findings indicate that the dust in Changchun snow primarily  
9 comprises clay aggregates (48%), quartz (22%), plagioclase (11%), calcite (6%), and  
10 orthoclase (5%), with no significant changes in the proportions of different mineral  
11 components during dry deposition processes. In contrast, wet deposition samples  
12 contain higher proportions of illite and quartz, which may be attributed to illite as an  
13 effective source of ice nuclei and the dynamic migration of quartz in snow. The study  
14 also found that the size and aspect ratio (AR) of dust follow normal distribution  
15 characteristics, with geometric means and standard deviations of 0.35-0.37  $\mu\text{m}$ , 1.88-  
16 2.12 for size, and 1.28-1.31, 1.22-1.23 for AR, respectively. Although there were no  
17 significant changes in the size and AR of dust during dry and wet deposition processes,  
18 significant variability was observed among different mineral component groups in  
19 terms of size and AR. Subsequently, based on statistically derived characteristics of dust  
20 components, size, and AR under observational constraints, we analyzed the light  
21 absorption characteristics of dust. The mass absorption cross-section ( $\text{MAC}_{\text{dust}}$ ) was  
22 found to be distributed within a narrow range ( $\sim 0\text{--}0.3 \text{ m}^2/\text{g}$ ). An increase in the relative



1 proportion of hematite was observed to increase  $MAC_{dust}$ , while an increase in dust  
2 particle size decreased  $MAC_{dust}$  by a specific percentage (10%-50%). Finally, the study  
3 discussed the complex effects of dust composition, particle size, concentration, and  
4 snow particle size on snow albedo. The results indicate that an increase in the relative  
5 proportion of hematite further enhances the reduction in snow albedo caused by dust,  
6 whereas an increase in dust particle size mitigates this reduction. Additionally, increases  
7 in dust concentration and snow particle size can further amplify these effects.

8 Compared with bulk sample collection and other techniques, we emphasize that  
9 CCSEM technology provides an innovative approach to detect the statistical  
10 characteristics of mineral composition, size distribution, and shape (AR) of dust in snow,  
11 significantly enhancing the accuracy of dust radiative forcing in model simulations.

12 However, it is worth noting that there is currently no strict set of criteria in the scientific  
13 community for classifying dust mineral components, making it difficult to compare dust  
14 composition reported in different literature, severely limiting research on dust chemical  
15 composition in different regions globally (Castellanos et al., 2024; Zhang et al., 2024).

16 Therefore, we call for the establishment of strict criteria for distinguishing mineral  
17 components as soon as possible, which will also support high-spectral projects and  
18 space programs developed and implemented by international societies and aerospace  
19 institutions to enhance understanding of mineral composition in terrestrial dust source  
20 regions (Green et al., 2020; Guanter et al., 2015). On the other hand, there is still a lack  
21 of understanding of the basic mineralogical and physical properties of dust particles,  
22 including key minerals such as hematite and goethite's spectral refractive indices.



1 Measurements of hematite refractive indices currently vary widely, hindering attempts  
2 to calculate dust optical properties and forcing changes (Zhang et al., 2024). In addition,  
3 the irregular shapes of dust particles cannot be represented by simple mathematical  
4 models, and the lack of comprehensive and realistic shape models is a prominent issue  
5 in dust optical modeling, distinguishing it from other aerosol types (Huang et al., 2023;  
6 Ito et al., 2021). Overall, the greatest limitation lies in the lack of detailed, region-  
7 specific, statistically representative information on the microphysical properties of base  
8 dust particles — size distribution, morphology, complex refractive index spectra,  
9 heterogeneity of internal structures, and resulting optical characteristics.

## 10 **Supporting Information**

11 Figures S1–S5.

12 Tables S1-S3

## 13 **Data availability statement**

14 The data used for analysis are available via a Zenodo archive, which can be found in  
15 the references (<https://zenodo.org/doi/10.5281/zenodo.14633496>, last access: 12 Jan  
16 2025).

## 17 **Author contributions**

18 X.W. and J.W. designed the study and evolved the overarching research goals and aims.  
19 T.S. wrote the first draft with contributions from all co-authors. T.S., Z.W., Y.Z. and  
20 W.P. collected snow samples and performed sampling analyses. T.S. and J.C. applied  
21 formal techniques such as statistical, mathematical and computational to analyze study





1 data. Y.B. and Z.H. provided the majority of the methodology and software. The other  
 2 authors provided technical guidance. All authors contributed to the improvement of  
 3 results and revised the final paper.

#### 4 **Competing interests**

5 The authors declare that they have no conflict of interest.

#### 6 **Financial support**

7 This research is jointly supported by the National Science Fund for Distinguished  
 8 Young Scholars (42025102), the Postdoctoral Fellowship Program of China  
 9 Postdoctoral Science Foundation (GZC20230674), the National Natural Science  
 10 Foundation of China (42375068, 42301142 and 42405099), and the Natural Science  
 11 Founds of Gansu Province, China (21ZDKA0017).

#### 12 **References**

- 13 Atkinson, J. D., Murray, B. J., Woodhouse, M. T., Whale, T. F., Baustian, K. J., Carslaw, K. S., Dobbie,  
 14 S., O'Sullivan, D., and Malkin, T. L.: The importance of feldspar for ice nucleation by mineral dust  
 15 in mixed-phase clouds, *Nature*, 498, 355-358, <https://doi.org/10.1038/nature12278>, 2013.
- 16 Bormann, K. J., McCabe, M. F., and Evans, J. P.: Satellite based observations for seasonal snow cover  
 17 detection and characterisation in Australia, *Remote Sens Environ*, 123, 57-71,  
 18 <https://doi.org/10.1016/j.rse.2012.03.003>, 2012.
- 19 Bormann, K. J., Brown, R. D., Derksen, C., and Painter, T. H.: Estimating snow-cover trends from space,  
 20 *Nat Clim Change*, 8, 923-927, <https://doi.org/10.1038/s41558-018-0318-3>, 2018.
- 21 Botet, R. S., and Rai, R. K.: Shape effects in optical properties of composite dust particles, *Earth Planets*  
 22 *Space*, 65, 1133-1137, <https://doi.org/10.5047/eps.2013.03.011>, 2013.
- 23 Bryant, A. C., Painter, T. H., Deems, J. S., and Bender, S. M.: Impact of dust radiative forcing in snow  
 24 on accuracy of operational runoff prediction in the Upper Colorado River Basin, *Geophys Res Lett*,  
 25 40, 3945-3949, <https://doi.org/10.1002/grl.50773>, 2013.
- 26 Castellanos, P., Colarco, P., Espinosa, W. R., Guzewich, S. D., Levy, R. C., Miller, R. L., Chin, M., Kahn,  
 27 R. A., Kemppinen, O., Moosmüller, H., Nowotnick, E. P., Rocha-Lima, A., Smith, M. D., Yorks, J.  
 28 E., and Yu, H.: Mineral dust optical properties for remote sensing and global modeling: A review,  
 29 *Remote Sens Environ*, 303, 113982, <https://doi.org/10.1016/j.rse.2023.113982>, 2024.



- 1 Chou, C., Formenti, P., Maille, M., Ausset, P., Helas, G., Harrison, M., and Osborne, S.: Size distribution,  
2 shape, and composition of mineral dust aerosols collected during the African Monsoon  
3 Multidisciplinary Analysis Special Observation Period 0: Dust and Biomass-Burning Experiment  
4 field campaign in Niger, January 2006, *Journal of Geophysical Research: Atmospheres*, 113,  
5 D00C10, <https://doi.org/10.1029/2008JD009897>, 2008.
- 6 Colarco, P. R., Nowottnick, E. P., Randles, C. A., Yi, B. Q., Yang, P., Kim, K. M., Smith, J. A., and  
7 Bardeen, C. G.: Impact of radiatively interactive dust aerosols in the NASA GEOS-5 climate model:  
8 Sensitivity to dust particle shape and refractive index, *J Geophys Res-Atmos*, 119, 753-786,  
9 <https://doi.org/10.1002/2013JD020046>, 2014.
- 10 Derksen, C., and Brown, R.: Spring snow cover extent reductions in the 2008-2012 period exceeding  
11 climate model projections, *Geophys Res Lett*, 39, L19504, <https://doi.org/10.1029/2012gl053387>,  
12 2012.
- 13 Derksen, C., Brown, R., Mudryk, L., and Luoju, K.: Terrestrial Snow Cover [in Arctic Report Card  
14 2017], [www.arctic.noaa.gov/reportcard](http://www.arctic.noaa.gov/reportcard), 162017.
- 15 Di Mauro, B., Fava, F., Ferrero, L., Garzonio, R., Baccolo, G., Delmonte, B., and Colombo, R.: Mineral  
16 dust impact on snow radiative properties in the European Alps combining ground, UAV, and satellite  
17 observations, *J Geophys Res-Atmos*, 120, 6080-6097, <https://doi.org/10.1002/2015jd023287>, 2015.
- 18 Doherty, S. J., Warren, S. G., Grenfell, T. C., Clarke, A. D., and Brandt, R. E.: Light-absorbing impurities  
19 in Arctic snow, *Atmos Chem Phys*, 10, 11647-11680, <https://doi.org/10.5194/acp-10-11647-2010>,  
20 2010.
- 21 Dong, Z. W., Brahney, J., Kang, S. C., Elser, J., Wei, T., Jiao, X. Y., and Shao, Y. P.: Aeolian dust transport,  
22 cycle and influences in high-elevation cryosphere of the Tibetan Plateau region: New evidences  
23 from alpine snow and ice, *Earth-Sci Rev*, 211, 103408,  
24 <https://doi.org/10.1016/j.earscirev.2020.103408>, 2020.
- 25 Dye, D. G.: Variability and trends in the annual snow-cover cycle in Northern Hemisphere land areas,  
26 1972-2000, *Hydrol Process*, 16, 3065-3077, <https://doi.org/10.1002/hyp.1089>, 2002.
- 27 Flanner, M. G., Arnheim, J. B., Cook, J. M., Dang, C., He, C., Huang, X., Singh, D., Skiles, S. M.,  
28 Whicker, C. A., and Zender, C. S.: SNICAR-ADv3: a community tool for modeling spectral snow  
29 albedo, *Geosci Model Dev*, 14, 7673-7704, <https://doi.org/10.5194/gmd-14-7673-2021>, 2021.
- 30 Formenti, P., Caquineau, S., Chevaillier, S., Klaver, A., Desboeufs, K., Rajot, J. L., Belin, S., and Briois,  
31 V.: Dominance of goethite over hematite in iron oxides of mineral dust from Western Africa:  
32 Quantitative partitioning by X-ray absorption spectroscopy, *J Geophys Res-Atmos*, 119, 12740-  
33 12754, <https://doi.org/10.1002/2014jd021668>, 2014.
- 34 Fountoulakis, I., Tsekeri, A., Kazadzis, S., Amiridis, V., Nersesian, A., Tsihla, M., Proestakis, E., Gkikas,  
35 A., Papachristopoulou, K., Barlakas, V., Emde, C., and Mayer, B.: A sensitivity study on radiative  
36 effects due to the parameterization of dust optical properties in models, *Atmos Chem Phys*, 24,  
37 4915-4948, <https://doi.org/10.5194/acp-24-4915-2024>, 2024.
- 38 Gardner, A. S., and Sharp, M. J.: A review of snow and ice albedo and the development of a new  
39 physically based broadband albedo parameterization, *Journal of Geophysical Research*, 115,  
40 F01009, <https://doi.org/10.1029/2009jf001444>, 2010.
- 41 Gasteiger, J., and Wiegner, M.: MOPSMAP v1.0: a versatile tool for the modeling of aerosol optical  
42 properties, *Geosci Model Dev*, 11, 2739-2762, <https://doi.org/10.5194/gmd-11-2739-2018>, 2018.
- 43 Gilardoni, S., Di Mauro, B., and Bonasoni, P.: Black carbon, organic carbon, and mineral dust in South  
44 American tropical glaciers: A review, *Global Planet Change*, 213, 103837,



- 1        <https://doi.org/10.1016/j.gloplacha.2022.103837>, 2022.
- 2    Go, S. J., Lyapustin, A., Schuster, G. L., Choi, M., Ginoux, P., Chin, M. A., Kalashnikova, O., Dubovik,
- 3        O., Kim, J., da Silva, A., Holben, B., and Reid, J. S.: Inferring iron-oxide species content in
- 4        atmospheric mineral dust from DSCOVR EPIC observations, *Atmos Chem Phys*, 22, 1395-1423,
- 5        <https://doi.org/10.5194/acp-22-1395-2022>, 2022.
- 6    González-Flórez, C., Klose, M., Alastuey, A., Dupont, S., Escribano, J., Etyemezian, V., Gonzalez-
- 7        Romero, A., Huang, Y., Kandler, K., Nikolich, G., Panta, A., Querol, X., Reche, C., Yus-Díez, J.,
- 8        and Pérez García-Pando, C.: Insights into the size-resolved dust emission from field measurements
- 9        in the Moroccan Sahara, *Atmos Chem Phys*, 23, 7177-7212, [https://doi.org/10.5194/acp-23-7177-](https://doi.org/10.5194/acp-23-7177-2023)
- 10        2023, 2023.
- 11    Green, R. O., Thompson, D. R., and Team, E.: An Earth Science Imaging Spectroscopy Mission: The
- 12        Earth Surface Mineral Dust Source Investigation (Emit), *Igarss 2020 - 2020 IEEE International*
- 13        *Geoscience and Remote Sensing Symposium*, 6262-6265,
- 14        <https://doi.org/10.1109/Igarss39084.2020.9323741>, 2020.
- 15    Guanter, L., Kaufmann, H., Segl, K., Foerster, S., Rogass, C., Chabrillat, S., Kuester, T., Hollstein, A.,
- 16        Rossner, G., Chlebek, C., Straif, C., Fischer, S., Schrader, S., Storch, T., Heiden, U., Mueller, A.,
- 17        Bachmann, M., Muhle, H., Muller, R., Habermeyer, M., Ohndorf, A., Hill, J., Buddenbaum, H.,
- 18        Hostert, P., van der Linden, S., Leitao, P. J., Rabe, A., Doerffer, R., Krasemann, H., Xi, H. Y., Mauser,
- 19        W., Hank, T., Locherer, M., Rast, M., Staenz, K., and Sang, B.: The EnMAP Spaceborne Imaging
- 20        Spectroscopy Mission for Earth Observation, *Remote Sens-Basel*, 7, 8830-8857,
- 21        <https://doi.org/10.3390/rs70708830>, 2015.
- 22    Haapanala, P., Raisanen, P., Kahnert, M., and Nousiainen, T.: Sensitivity of the shortwave radiative effect
- 23        of dust on particle shape: Comparison of spheres and spheroids, *J Geophys Res-Atmos*, 117,
- 24        D08201, <https://doi.org/10.1029/2011jd017216>, 2012.
- 25    Hadley, O. L., and Kirchstetter, T. W.: Black-carbon reduction of snow albedo, *Nat Clim Change*, 2, 437-
- 26        440, <https://doi.org/10.1038/nclimate1433>, 2012.
- 27    Hall, D. K., Riggs, G. A., and Salomonson, V. V.: Development of Methods for Mapping Global Snow
- 28        Cover Using Moderate Resolution Imaging Spectroradiometer Data, *Remote Sens Environ*, 54, 127-
- 29        140, [https://doi.org/10.1016/0034-4257\(95\)00137-P](https://doi.org/10.1016/0034-4257(95)00137-P), 1995.
- 30    Hall, D. K., Crawford, C. J., DiGirolamo, N. E., Riggs, G. A., and Foster, J. L.: Detection of earlier
- 31        snowmelt in the Wind River Range, Wyoming, using Landsat imagery, 1972–2013, *Remote Sens*
- 32        *Environ*, 162, 45-54, <https://doi.org/10.1016/j.rse.2015.01.032>, 2015.
- 33    Hansen, J., and Nazarenko, L.: Soot climate forcing via snow and ice albedos, *P Natl Acad Sci USA*, 101,
- 34        423-428, <https://doi.org/10.1073/pnas.2237157100>, 2004.
- 35    Hao, D., Bisht, G., Wang, H., Xu, D., Huang, H., Qian, Y., and Leung, L. R.: A cleaner snow future
- 36        mitigates Northern Hemisphere snowpack loss from warming, *Nat Commun*, 14, 6074,
- 37        <https://doi.org/10.1038/s41467-023-41732-6>, 2023.
- 38    Harrison, A. D., O'Sullivan, D., Adams, M. P., Porter, G. C. E., Blades, E., Brathwaite, C., Chewitt-Lucas,
- 39        R., Gaston, C., Hawker, R., Krüger, O. O., Neve, L., Pöhlker, M. L., Pöhlker, C., Pöschl, U.,
- 40        Sanchez-Marroquin, A., Sealy, A., Sealy, P., Tarn, M. D., Whitehall, S., McQuaid, J. B., Carslaw, K.
- 41        S., Prospero, J. M., and Murray, B. J.: The ice-nucleating activity of African mineral dust in the
- 42        Caribbean boundary layer, *Atmos Chem Phys*, 22, 9663-9680, [https://doi.org/10.5194/acp-22-9663-](https://doi.org/10.5194/acp-22-9663-2022)
- 43        2022, 2022.
- 44    He, C., and Flanner, M.: Snow Albedo and Radiative Transfer: Theory, Modeling, and Parameterization,



- 1 in: Springer Series in Light Scattering: Volume 5: Radiative Transfer, Remote Sensing, and Light
- 2 Scattering, edited by: Kokhanovsky, A., Springer International Publishing, Cham, 67-133, 2020.
- 3 He, C., Flanner, M., Lawrence, D. M., and Gu, Y.: New Features and Enhancements in Community Land
- 4 Model (CLM5) Snow Albedo Modeling: Description, Sensitivity, and Evaluation, *J Adv Model*
- 5 *Earth Sy*, 16, e2023MS003861, <https://doi.org/10.1029/2023MS003861>, 2024.
- 6 Huang, J. P., Yu, H. P., Guan, X. D., Wang, G. Y., and Guo, R. X.: Accelerated dryland expansion under
- 7 climate change, *Nat Clim Change*, 6, 166-171, <https://doi.org/10.1038/Nclimate2837>, 2016.
- 8 Huang, Y., Kok, J. F., Saito, M., and Munoz, O.: Single-scattering properties of ellipsoidal dust aerosols
- 9 constrained by measured dust shape distributions, *Atmos Chem Phys*, 23, 2557-2577,
- 10 <https://doi.org/10.5194/acp-23-2557-2023>, 2023.
- 11 Immerzeel, W. W., Droogers, P., de Jong, S. M., and Bierkens, M. F. P.: Large-scale monitoring of snow
- 12 cover and runoff simulation in Himalayan river basins using remote sensing, *Remote Sens Environ*,
- 13 113, 40-49, <https://doi.org/10.1016/j.rse.2008.08.010>, 2009.
- 14 Ito, A., Adebisi, A. A., Huang, Y., and Kok, J. F.: Less atmospheric radiative heating by dust due to the
- 15 synergy of coarser size and aspherical shape, *Atmos Chem Phys*, 21, 16869-16891,
- 16 <https://doi.org/10.5194/acp-21-16869-2021>, 2021.
- 17 Kahnert, M.: Modelling radiometric properties of inhomogeneous mineral dust particles: Applicability
- 18 and limitations of effective medium theories, *J Quant Spectrosc Ra*, 152, 16-27,
- 19 <https://doi.org/10.1016/j.jqsrt.2014.10.025>, 2015.
- 20 Kandler, K., Benker, N., Bundke, U., Cuevas, E., Ebert, M., Knippertz, P., Rodriguez, S., Schütz, L., and
- 21 Weinbruch, S.: Chemical composition and complex refractive index of Saharan Mineral Dust at
- 22 Izana, Tenerife (Spain) derived by electron microscopy, *Atmospheric Environment*, 41, 8058-8074,
- 23 <https://doi.org/10.1016/j.atmosenv.2007.06.047>, 2007.
- 24 Kandler, K., Schütz, L., Deutscher, C., Ebert, M., Hofmann, H., Jäckel, S., Jaenicke, R., Knippertz, P.,
- 25 Lieke, K., Massling, A., Petzold, A., Schladitz, A., Weinzierl, B., Wiedensohler, A., Zorn, S., and
- 26 Weinbruch, S.: Size distribution, mass concentration, chemical and mineralogical composition and
- 27 derived optical parameters of the boundary layer aerosol at Tinfou, Morocco, during SAMUM 2006,
- 28 *Tellus B*, 61, 32-50, <https://doi.org/10.1111/j.1600-0889.2008.00385.x>, 2009.
- 29 Kang, S., Zhang, Y., Qian, Y., and Wang, H.: A review of black carbon in snow and ice and its impact on
- 30 the cryosphere, *Earth-Sci Rev*, 210, 103346, <https://doi.org/10.1016/j.earscirev.2020.103346>, 2020.
- 31 Kanngiesser, F., and Kahnert, M.: Modeling Optical Properties of Non-Cubical Sea-Salt Particles, *J*
- 32 *Geophys Res-Atmos*, 126, e2020JD033674, <https://doi.org/10.1029/2020JD033674>, 2021.
- 33 Kaspari, S., Skiles, S. M., Delaney, I., Dixon, D., and Painter, T. H.: Accelerated glacier melt on Snow
- 34 Dome, Mount Olympus, Washington, USA, due to deposition of black carbon and mineral dust from
- 35 wildfire, *J Geophys Res-Atmos*, 120, 2793-2807, <https://doi.org/10.1002/2014jd022676>, 2015.
- 36 Kok, J. F.: A scaling theory for the size distribution of emitted dust aerosols suggests climate models
- 37 underestimate the size of the global dust cycle, *P Natl Acad Sci USA*, 108, 1016-1021,
- 38 <https://doi.org/10.1073/pnas.1014798108>, 2011.
- 39 Kok, J. F., Ridley, D. A., Zhou, Q., Miller, R. L., Zhao, C., Heald, C. L., Ward, D. S., Albani, S., and
- 40 Haustein, K.: Smaller desert dust cooling effect estimated from analysis of dust size and abundance,
- 41 *Nat Geosci*, 10, 274-278, <https://doi.org/10.1038/Ngeo2912>, 2017.
- 42 Kuchiki, K., Aoki, T., Niwano, M., Matoba, S., Kodama, Y., and Adachi, K.: Elemental carbon, organic
- 43 carbon, and dust concentrations in snow measured with thermal optical and gravimetric methods:
- 44 Variations during the 2007–2013 winters at Sapporo, Japan, *Journal of Geophysical Research:*



- 1 Atmospheres, 120, 868-882, <https://doi.org/10.1002/2014JD022144>, 2015.
- 2 Lee, K. M., Choi, H., and Kim, J.: Refractive Index for Asian Dust in the Ultraviolet - Visible Region
- 3 Determined From Compositional Analysis 3 and Validated With OMI Observations, *J Geophys Res-*
- 4 *Atmos*, 125, e2019JD030629, <https://doi.org/10.1029/2019JD030629>, 2020.
- 5 Lemke, P., Ren, J., Alley, R. B., Allison, I., Carrasco, J., Flato, G., Fujii, Y., Kaser, G., Mote, P., and
- 6 Thomas, R. H.: Observations: Changes in Snow, Ice and Frozen Ground, *Climate Change 2007:*
- 7 *The Physical Science Basis. Contribution of Working Group I to the Fourth Assessment Report of*
- 8 *the Intergovernmental Panel on Climate Change*, 2007.
- 9 Li, L., Mahowald, N. M., Gonçalves Ageitos, M., Obiso, V., Miller, R. L., Pérez García-Pando, C., Di
- 10 Biagio, C., Formenti, P., Brodrick, P. G., Clark, R. N., Green, R. O., Kokaly, R., Swayze, G., and
- 11 Thompson, D. R.: Improved constraints on hematite refractive index for estimating climatic effects
- 12 of dust aerosols, *Communications Earth & Environment*, 5, 295, [https://doi.org/10.1038/s43247-](https://doi.org/10.1038/s43247-024-01441-4)
- 13 [024-01441-4](https://doi.org/10.1038/s43247-024-01441-4), 2024.
- 14 Li, Y., Kang, S., Zhang, X., Chen, J., Schmale, J., Li, X., Zhang, Y., Niu, H., Li, Z., Qin, X., He, X., Yang,
- 15 W., Zhang, G., Wang, S., Shao, L., and Tian, L.: Black carbon and dust in the Third Pole glaciers:
- 16 Revaluated concentrations, mass absorption cross-sections and contributions to glacier ablation, *Sci*
- 17 *Total Environ*, 789, 147746, <https://doi.org/10.1016/j.scitotenv.2021.147746>, 2021.
- 18 Mote, P. W., Li, S. H., Lettenmaier, D. P., Xiao, M., and Engel, R.: Dramatic declines in snowpack in the
- 19 western US, *Npj Climate and Atmospheric Science*, 1, 2, [https://doi.org/10.1038/s41612-018-0012-](https://doi.org/10.1038/s41612-018-0012-1)
- 20 [1](https://doi.org/10.1038/s41612-018-0012-1), 2018.
- 21 Moteki, N., Adachi, K., Ohata, S., Yoshida, A., Harigaya, T., Koike, M., and Kondo, Y.: Anthropogenic
- 22 iron oxide aerosols enhance atmospheric heating, *Nat Commun*, 8, 15329,
- 23 <https://doi.org/10.1038/ncomms15329>, 2017.
- 24 Neff, J. C., Ballantyne, A. P., Farmer, G. L., Mahowald, N. M., Conroy, J. L., Landry, C. C., Overpeck,
- 25 J. T., Painter, T. H., Lawrence, C. R., and Reynolds, R. L.: Increasing eolian dust deposition in the
- 26 western United States linked to human activity, *Nat Geosci*, 1, 189-195,
- 27 <https://doi.org/10.1038/ngeo133>, 2008.
- 28 Okada, K., Heintzenberg, J., Kai, K. J., and Qin, Y.: Shape of atmospheric mineral particles collected in
- 29 three Chinese arid-regions, *Geophys Res Lett*, 28, 3123-3126,
- 30 <https://doi.org/10.1029/2000gl012798>, 2001.
- 31 Painter, T. H., Skiles, S. M., Deems, J. S., Bryant, A. C., and Landry, C. C.: Dust radiative forcing in
- 32 snow of the Upper Colorado River Basin: 1. A 6 year record of energy balance, radiation, and dust
- 33 concentrations, *Water Resour Res*, 48, W07521, <https://doi.org/10.1029/2012WR011985>, 2012.
- 34 Panta, A., Kandler, K., Alastuey, A., González-Flórez, C., González-Romero, A., Klose, M., Querol, X.,
- 35 Reche, C., Yus-Díez, J., and Pérez García-Pando, C.: Insights into the single-particle composition,
- 36 size, mixing state, and aspect ratio of freshly emitted mineral dust from field measurements in the
- 37 Moroccan Sahara using electron microscopy, *Atmos Chem Phys*, 23, 3861-3885,
- 38 <https://doi.org/10.5194/acp-23-3861-2023>, 2023.
- 39 Prakash, P. J., Stenchikov, G., Tao, W. C., Yapici, T., Warsama, B., and Engelbrecht, J. P.: Arabian Red
- 40 Sea coastal soils as potential mineral dust sources, *Atmos Chem Phys*, 16, 11991-12004,
- 41 <https://doi.org/10.5194/acp-16-11991-2016>, 2016.
- 42 Pulliainen, J., Luojus, K., Derksen, C., Mudryk, L., Lemmetyinen, J., Salminen, M., Ikonen, J., Takala,
- 43 M., Cohen, J., Smolander, T., and Norberg, J.: Patterns and trends of Northern Hemisphere snow
- 44 mass from 1980 to 2018, *Nature*, 581, 294-298, <https://doi.org/10.1038/s41586-020-2258-0>, 2020.



- 1 Réveillet, M., Dumont, M., Gascoin, S., Lafaysse, M., Nabat, P., Ribes, A., Nheili, R., Tuzet, F., Ménégouz,  
2 M., Morin, S., Picard, G., and Ginoux, P.: Black carbon and dust alter the response of mountain  
3 snow cover under climate change, *Nat Commun*, 13, 5279, [https://doi.org/10.1038/s41467-022-](https://doi.org/10.1038/s41467-022-32501-y)  
4 32501-y, 2022.
- 5 Reynolds, R. L., Goldstein, H. L., Moskowitz, B. M., Kokaly, R. F., Munson, S. M., Solheid, P., Breit,  
6 G. N., Lawrence, C. R., and Derry, J.: Dust Deposited on Snow Cover in the San Juan Mountains,  
7 Colorado, 2011-2016: Compositional Variability Bearing on Snow-Melt Effects, *J Geophys Res-*  
8 *Atmos*, 125, e2019JD032210, <https://doi.org/10.1029/2019JD032210>, 2020.
- 9 Rocha-Lima, A., Martins, J. V., Remer, L. A., Todd, M., Marsham, J. H., Engelstaedter, S., Ryder, C. L.,  
10 Cavazos-Guerra, C., Artaxo, P., Colarco, P., and Washington, R.: A detailed characterization of the  
11 Saharan dust collected during the Fennec campaign in 2011: in situ ground-based and laboratory  
12 measurements, *Atmos Chem Phys*, 18, 1023-1043, <https://doi.org/10.5194/acp-18-1023-2018>, 2018.
- 13 Ryder, C. L., Marengo, F., Brooke, J. K., Estelles, V., Cotton, R., Formenti, P., McQuaid, J. B., Price, H.  
14 C., Liu, D. T., Ausset, P., Rosenberg, P. D., Taylor, J. W., Choularton, T., Bower, K., Coe, H.,  
15 Gallagher, M., Crosier, J., Lloyd, G., Highwood, E. J., and Murray, B. J.: Coarse-mode mineral dust  
16 size distributions, composition and optical properties from AER-D aircraft measurements over the  
17 tropical eastern Atlantic, *Atmos Chem Phys*, 18, 17225-17257, [https://doi.org/10.5194/acp-18-](https://doi.org/10.5194/acp-18-17225-2018)  
18 17225-2018, 2018.
- 19 Sarangi, C., Qian, Y., Rittger, K., Leung, L. R., Chand, D., Bormann, K. J., and Painter, T. H.: Dust  
20 dominates high-altitude snow darkening and melt over high-mountain Asia, *Nat Clim Change*, 10,  
21 1045-1051, <https://doi.org/10.1038/s41558-020-00909-3>, 2020.
- 22 Shi, T., Cui, J., Chen, Y., Zhou, Y., Pu, W., Xu, X., Chen, Q., Zhang, X., and Wang, X.: Enhanced light  
23 absorption and reduced snow albedo due to internally mixed mineral dust in grains of snow, *Atmos*  
24 *Chem Phys*, 21, 6035-6051, <https://doi.org/10.5194/acp-21-6035-2021>, 2021.
- 25 Shi, T., He, C., Zhang, D., Zhang, X., Niu, X., Xing, Y., Chen, Y., Cui, J., Pu, W., and Wang, X.: Opposite  
26 Effects of Mineral Dust Nonsphericity and Size on Dust-Induced Snow Albedo Reduction, *Geophys*  
27 *Res Lett*, 49, e2022GL099031, <https://doi.org/10.1029/2022GL099031>, 2022.
- 28 Shi, Z. B., Shao, L. T., Jones, T. P., and Lu, S. L.: Microscopy and mineralogy of airborne particles  
29 collected during severe dust storm episodes in Beijing, China, *J Geophys Res-Atmos*, 110, D01303,  
30 <https://doi.org/10.1029/2004jd005073>, 2005.
- 31 Skiles, S. M., Flanner, M., Cook, J. M., Dumont, M., and Painter, T. H.: Radiative forcing by light-  
32 absorbing particles in snow, *Nat Clim Change*, 8, 964-971, [https://doi.org/10.1038/s41558-018-](https://doi.org/10.1038/s41558-018-0296-5)  
33 0296-5, 2018.
- 34 Song, Q. Q., Zhang, Z. B., Yu, H. B., Kok, J. F., Di Biagio, C., Albani, S., Zheng, J. Y., and Ding, J. C.:  
35 Size-resolved dust direct radiative effect efficiency derived from satellite observations, *Atmos*  
36 *Chem Phys*, 22, 13115-13135, <https://doi.org/10.5194/acp-22-13115-2022>, 2022.
- 37 Tan, X. J., Wu, Z. N., Mu, X. M., Gao, P., Zhao, G. J., Sun, W. Y., and Gu, C. J.: Spatiotemporal changes  
38 in snow cover over China during 1960-2013, *Atmos Res*, 218, 183-194,  
39 <https://doi.org/10.1016/j.atmosres.2018.11.018>, 2019.
- 40 Thackeray, C. W., Fletcher, C. G., Mudryk, L. R., and Derksen, C.: Quantifying the Uncertainty in  
41 Historical and Future Simulations of Northern Hemisphere Spring Snow Cover, *J Climate*, 29, 8647-  
42 8663, <https://doi.org/10.1175/Jcli-D-16-0341.1>, 2016.
- 43 Wang, X., Pu, W., Ren, Y., Zhang, X., Zhang, X., Shi, J., Jin, H., Dai, M., and Chen, Q.: Observations  
44 and model simulations of snow albedo reduction in seasonal snow due to insoluble light-absorbing



- 1 particles during 2014 Chinese survey, *Atmos Chem Phys*, 17, 2279-2296,
- 2 <https://doi.org/10.5194/acp-17-2279-2017>, 2017.
- 3 Wang, X., Zhang, C., Shi, T., Zhang, D., Zhao, P., and Zhao, P.: Case Investigation on the Influence of
- 4 In-Snow Particles' Size and Composition on the Snow Light Absorption and Albedo, *Geophys Res*
- 5 *Lett*, 50, e2023GL103362, <https://doi.org/10.1029/2023GL103362>, 2023.
- 6 Winton, V. H. L., Charlier, B. L. A., Jolly, B. H., Purdie, H., Anderson, B., Hunt, J. E., Dadic, R., Taylor,
- 7 S., Petherick, L., and Novis, P. M.: New Zealand Southern Alps Blanketed by Red Australian Dust
- 8 During 2019/2020 Severe Bushfire and Dust Event, *Geophys Res Lett*, 51, e2024GL112782,
- 9 <https://doi.org/10.1029/2024GL112782>, 2024.
- 10 Xie, X. N., Liu, X. D., Che, H. Z., Xie, X. X., Li, X. Z., Shi, Z. G., Wang, H. L., Zhao, T. L., and Liu, Y.
- 11 G.: Radiative feedbacks of dust in snow over eastern Asia in CAM4-BAM, *Atmos Chem Phys*, 18,
- 12 12683-12698, <https://doi.org/10.5194/acp-18-12683-2018>, 2018.
- 13 Xing, Y., Chen, Y., Yan, S., Cao, X., Zhou, Y., Zhang, X., Shi, T., Niu, X., Wu, D., Cui, J., Zhou, Y., Wang,
- 14 X., and Pu, W.: Dust storms from the Taklamakan Desert significantly darken snow surface on
- 15 surrounding mountains, *Atmos. Chem. Phys.*, 24, 5199-5219, [https://doi.org/10.5194/acp-24-5199-](https://doi.org/10.5194/acp-24-5199-2024)
- 16 2024, 2024.
- 17 Yu, Y., and Ginoux, P.: Enhanced dust emission following large wildfires due to vegetation disturbance,
- 18 *Nat Geosci*, 15, 878-884, <https://doi.org/10.1038/s41561-022-01046-6>, 2022.
- 19 Zeng, X. B., Broxton, P., and Dawson, N.: Snowpack Change From 1982 to 2016 Over Conterminous
- 20 United States, *Geophys Res Lett*, 45, 12940-12947, <https://doi.org/10.1029/2018gl079621>, 2018.
- 21 Zhang, X. L., Wu, G. J., Zhang, C. L., Xu, T. L., and Zhou, Q. Q.: What is the real role of iron oxides in
- 22 the optical properties of dust aerosols?, *Atmos Chem Phys*, 15, 12159-12177,
- 23 <https://doi.org/10.5194/acp-15-12159-2015>, 2015.
- 24 Zhang, Y., Saito, M., Yang, P., Schuster, G., and Trepte, C.: Sensitivities of Spectral Optical Properties
- 25 of Dust Aerosols to Their Mineralogical and Microphysical Properties, *Journal of Geophysical*
- 26 *Research: Atmospheres*, 129, e2023JD040181, <https://doi.org/10.1029/2023JD040181>, 2024.
- 27 Zhang, Y. L., Kang, S. C., Sprenger, M., Cong, Z. Y., Gao, T. G., Li, C. L., Tao, S., Li, X. F., Zhong, X.
- 28 Y., Xu, M., Meng, W. J., Neupane, B., Qin, X., and Sillanpaa, M.: Black carbon and mineral dust in
- 29 snow cover on the Tibetan Plateau, *Cryosphere*, 12, 413-431, [https://doi.org/10.5194/tc-12-413-](https://doi.org/10.5194/tc-12-413-2018)
- 30 2018, 2018.
- 31 Zhao, P., Zhao, P., Tang, J., Casuccio, G. S., Gao, J., Li, J., He, Y., Li, M., and Feng, Y.: Source
- 32 identification and apportionment of ambient particulate matter in Beijing using an advanced
- 33 computer-controlled scanning electron microscopy (CCSEM) system, *Sci Total Environ*, 861,
- 34 160608, <https://doi.org/10.1016/j.scitotenv.2022.160608>, 2022.
- 35 Zhu, X., Lee, S. Y., Wen, X. H., Wei, Z. G., Ji, Z. M., Zheng, Z. Y., and Dong, W. J.: Historical evolution
- 36 and future trend of Northern Hemisphere snow cover in CMIP5 and CMIP6 models, *Environmental*
- 37 *Research Letters*, 16, 065013, <https://doi.org/10.1088/1748-9326/ac0662>, 2021.
- 38